AGU PUBLICATIONS

JGR

Journal of Geophysical Research: Oceans

RESEARCH ARTICLE

10.1002/2014JC010292

Key Points:
- Anticyclonic (cyclonic) eddies generate negative (positive) *p*CFC-11 anomalies
- Mixed layer dynamics is the key process that modulates the surface *p*CFC-11
- Anticyclones lead to a slight increase in the net uptake of CFC-11

Correspondence to:
H. Song,
hajsong@mit.edu

Citation:
Song, H., J. Marshall, P. Gaube, and D. J. McGillicuddy (2015), Anomalous chlorofluorocarbon uptake by mesoscale eddies in the Drake Passage region, *J. Geophys. Res. Oceans*, *120*, 1065–1078, doi:10.1002/2014JC010292.

Received 7 JUL 2014
Accepted 2 JAN 2015
Accepted article online 8 JAN 2015
Published online 23 FEB 2015

Anomalous chlorofluorocarbon uptake by mesoscale eddies in the Drake Passage region

Hajoon Song[1], John Marshall[1], Peter Gaube[2], and Dennis J. McGillicuddy Jr[2]

[1]Department of Earth, Atmospheric and Planetary Sciences, Massachusetts Institute of Technology, Cambridge, Massachusetts, USA, [2]Department of Applied Ocean Physics and Engineering, Woods Hole Oceanographic Institution, Woods Hole, Massachusetts, USA

Abstract The role of mesoscale eddies in the uptake of anthropogenic chlorofluorocarbon-11 (CFC-11) gas is investigated with a 1/20° eddy-resolving numerical ocean model of a region of the Southern Ocean. With a relatively fast air-sea equilibrium time scale (about a month), the air-sea CFC-11 flux quickly responds to the changes in the mixed layer CFC-11 partial pressure (*p*CFC-11). At the mesoscale, significant correlations are observed between *p*CFC-11 anomaly, anomalies in sea surface temperature (SST), net heat flux, and mixed layer depth. An eddy-centric analysis of the simulated CFC-11 field suggests that anticyclonic warm-core eddies generate negative *p*CFC-11 anomalies and cyclonic cold-core eddies generate positive anomalies of *p*CFC-11. Surface *p*CFC-11 is modulated by mixed layer dynamics in addition to CFC-11 air-sea fluxes. A negative cross correlation between mixed layer depth and surface *p*CFC-11 anomalies is linked to higher CFC-11 uptake in anticyclones and lower CFC-11 uptake in cyclones, especially in winter. An almost exact asymmetry in the air-sea CFC-11 flux between cyclones and anticyclones is found.

1. Introduction

Mesoscale eddies, coherent features with radius scales of O (100 km), play a major role in the general circulation of the ocean and marine ecosystem dynamics. In the open ocean, they can enhance productivity by supplying nutrients from the interior to the euphotic zone [*McGillicuddy et al*., 1998; *Oschlies*, 2002]. In the eastern boundary upwelling system, in contrast, they tend to suppress nearshore biological activity by transporting nutrients to the open ocean [*Lathuilière et al*., 2010; *Gruber et al*., 2011]. Their role in local ecosystem dynamics depends on their polarity (cyclonic versus anticyclonic), region of formation, and whether they are intensifying or decaying [*McGillicuddy et al*., 1998, 2007; *Gaube et al*., 2013].

Anomalous features in mesoscale eddies can also modulate air-sea heat and gases fluxes. Warmer or cooler sea surface temperatures (SST) associated with eddies can influence air-sea heat fluxes. For example, if surface air temperature is in equilibrium with the ambient mean SST, sensible heat flux would cause warm eddies to lose buoyancy and become less stratified while cold eddies would become more stratified with buoyancy gain. Similarly, air-sea gas fluxes can be anomalous in mesoscale eddies. With a relatively uniform distribution of gases in the atmosphere, anomalous air-sea gas fluxes can occur when the concentration at the ocean surface is modulated by variations in solubility and vertical mixing which in turn are affected by SST and upper ocean stratification, respectively.

Chlorofluorocarbon-11 (CFC-11) is an anthropogenic gas that was introduced in the 1940s [*Walker et al*., 2000]. With rapid air-sea gas exchange, the surface ocean can reach equilibrium with atmospheric partial CFC-11 pressure (*p*CFC-11) in roughly 1 month because of the absence of buffer factors [*Ito et al*., 2004]. Once entering the ocean, CFC-11 is advected and diffused by ocean currents, thereby serving as a tracer for ocean ventilation processes [*Fine*, 2011]. Because its distribution is controlled by conservative processes, it is much easier to understand than biogeochemically active gases and therefore provides an ideal reference to study the role of eddies in modulating air-sea gas fluxes.

Global CFC-11 observations began in the 1990s as part of the World Ocean Circulation Experiment (WOCE) and continued with the Climate Variability and Predictability (CLIVAR) repeat hydrography program. These observations clearly highlight the role of intermediate and mode waters and suggest that the Southern Ocean is one of the biggest sinks for CFC-11 and other anthropogenic gases [*Key et al*., 2004]. Observations

of CFC-12, another inert anthropogenic tracer, have also been used to estimate changes in ocean ventilation processes [*Hartin et al*., 2011; *Waugh et al*., 2013].

Global observations of CFC-11 can be used to evaluate ocean ventilation processes in numerical models [*England*, 1995; *Dixon et al*., 1996; *England and Hirst*, 1997; *England and Maier-Reimer*, 2001; *Müller et al*., 2006; *Trossman et al*., 2012]. With known atmospheric forcing, zero initial concentration, and passive tracer behavior in the ocean, modeling CFC-11 is relatively easy and widely performed. As part of the Ocean Carbon-cycle Model Intercomparison Project second phase (OCMIP-2), 13 ocean circulation models simulated CFC-11 allowing their ventilation process as represented by CFC-11 distribution in the ocean to be compared to the observations [*Dutay et al*., 2002]. CFC-11 can also be used to examine the role of mesoscale eddies in modulating ocean ventilation processes [*Lachkar et al*., 2007; *Booth and Kamenkovich*, 2008]. Resolving eddies often improves the representation of ventilation in ocean models because eddies tend to restratify the upper ocean, thereby reducing uptake. This restratification is often underestimated in models that do not resolve eddies [*Lachkar et al*., 2007]. In addition, simulation of CFC-11 is useful to understand a model's ventilation processes before exploring uptake of anthropogenic CO_2. For example, *Long et al*. [2013] have made use of CFC-11 to quantify mode and intermediate water formation in the Southern Ocean and determine that it is underestimated, leading to negative biases in anthropogenic CFC-11 and CO_2 uptake.

Because CFC-11 can be used to evaluate transient tracer air-sea fluxes without the additional complications imposed by biological processes, we investigate the roles of cyclonic and anticyclonic eddies in CFC-11 uptake and their net effect on total CFC-11 uptake here. Using an automated eddy detection technique, mesoscale eddies are first identified from the high-resolution numerical model configured over the Southern Ocean. We then compute the surface *p*CFC-11 anomalies and CFC-11 air-sea flux anomalies. These computations allow us to test our hypothesis that anomalous vertical mixing by eddies causes the CFC-11 flux anomalies, and to quantify the net effect of eddies on CFC-11 uptake. We find that deeper mixed layers in anticyclones result in more CFC-11 uptake, whereas uptake is less than the mean in cyclones. We also find that positive anomalies in CFC-11 uptake in anticyclones are mostly canceled out by negative anomalies in cyclones, although the net eddy-induced uptake is slightly positive.

This paper is organized as follows. The description of the ocean model, eddy-centric diagnostic method, and CFC-11 flux analysis are provided in section 2. Section 3 presents the simulated *p*CFC-11 and CFC-11 flux in the eddy-resolving ocean model, focusing on the role of mesoscale eddies, and their contribution to CFC-11 flux in a sector of the Southern Ocean. A general discussion then follows to conclude in section 4.

2. CFC-11 Simulation With an Eddy-Resolving Ocean Model

2.1. High-Resolution Simulation of the "DIMES Patch"

We use the eddy-resolving Massachusetts Institute of Technology General Circulation Model (MITgcm) [*Marshall et al*., 1997b, 1997a; *Adcroft et al*., 1997; *Marshall et al*., 1998; *Adcroft et al*., 1999] with very high horizontal resolution (1/20°) over the Drake Passage. It covers more than one third of entire Antarctic Circumpolar Current (ACC), ranging from 160°W to 20°W and from 75°S to 35°S (Figure 1). The model configuration is the same as that used to estimate the lateral eddy diffusivity upstream of Drake Passage [*Tulloch et al*., 2014; *LaCasce et al*., 2014], except that 50 vertical levels are used in this study instead of 100 levels. The vertical resolution of the upper 200 m of the ocean is on the order of 10 m. The boundary conditions for hydrodynamic state variables and tracers including CFC-11 were extracted from a lower resolution (1° in the horizontal) global model that was integrated with atmospheric CFC-11 forcing up to 1998. The 1/20° regional model is integrated from 1990 to 1994 with those boundary conditions and interannual Common Ocean-ice Reference Experiments version 2 (CORE-II) surface forcing. The details of the model settings, surface, and boundary forcing are provided in Appendix A.

2.2. CFC-11 Flux

The atmosphere is the only source for CFC-11, and it enters the ocean through the surface. Following the OCMIP-2 protocol, the air-sea gas flux for CFC-11 (F_{CFC-11}) is modeled as follows:

$$F_{CFC-11} = K_w (C_{sat} - C), \tag{1}$$

where K_w is the parameterized gas transfer velocity (m s^{-1}) which is a function of SST and the square of the wind speed, following *Wanninkhof* [1992]. The C_{sat} is the *p*CFC-11 at saturation with the atmospheric value

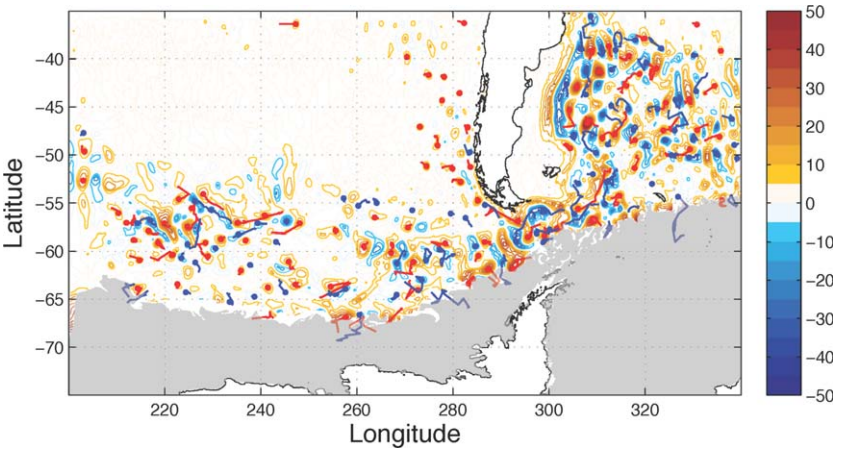

Figure 1. Eddies (dots) detected from SSH anomaly fields (colored contours with 5 cm interval with color scale on the right) in winter. Red (blue) dots represent the anticyclonic (cyclonic) eddy locations, and their sizes are proportionally scaled by the radius of a circle whose area is equal to that of the enclosed outer most SSH anomaly contour. Red and blue lines are trajectories of eddies whose life cycles are longer than 1 week. Sea ice coverage is marked in gray.

computed following *Warner and Weiss* [1985], and C is the oceanic pCFC-11 at the surface that is a function of the CFC-11 concentration, temperature, and salinity. If the surface ocean is undersaturated with respect to the atmospheric value (C is lower than C_{sat}), then CFC-11 enters the ocean at a rate set by K_w and the air-sea concentration gradient. The effects of a typical SST anomaly in eddies (1°C) on F_{CFC-11} are 2 orders of magnitude smaller than that of a surface pCFC-11 anomaly (3 patm). Because the equilibrium time scale for CFC-11 is roughly 1 month, the surface ocean is close to equilibrium with atmospheric pCFC-11. Accordingly, little spatial variability of pCFC-11 is observed at the surface in most places. In the Southern Ocean, however, pCFC-11 decreases poleward slightly, yielding a meridional gradient of surface pCFC-11 [*Key et al.*, 2004]. Additionally, undersaturation of pCFC-11 can occur when vertical mixing decreases the surface value by dilution with subsurface water that is undersaturated with respect to pCFC-11 [*Haine and Richards*, 1995; *Shao et al.*, 2013]. The pCFC-11 simulation also visually shows the inverse correlation between mixed layer depth (MLD) and surface pCFC-11 (Figure 2). For a given K_w, the CFC-11 flux depends on the difference

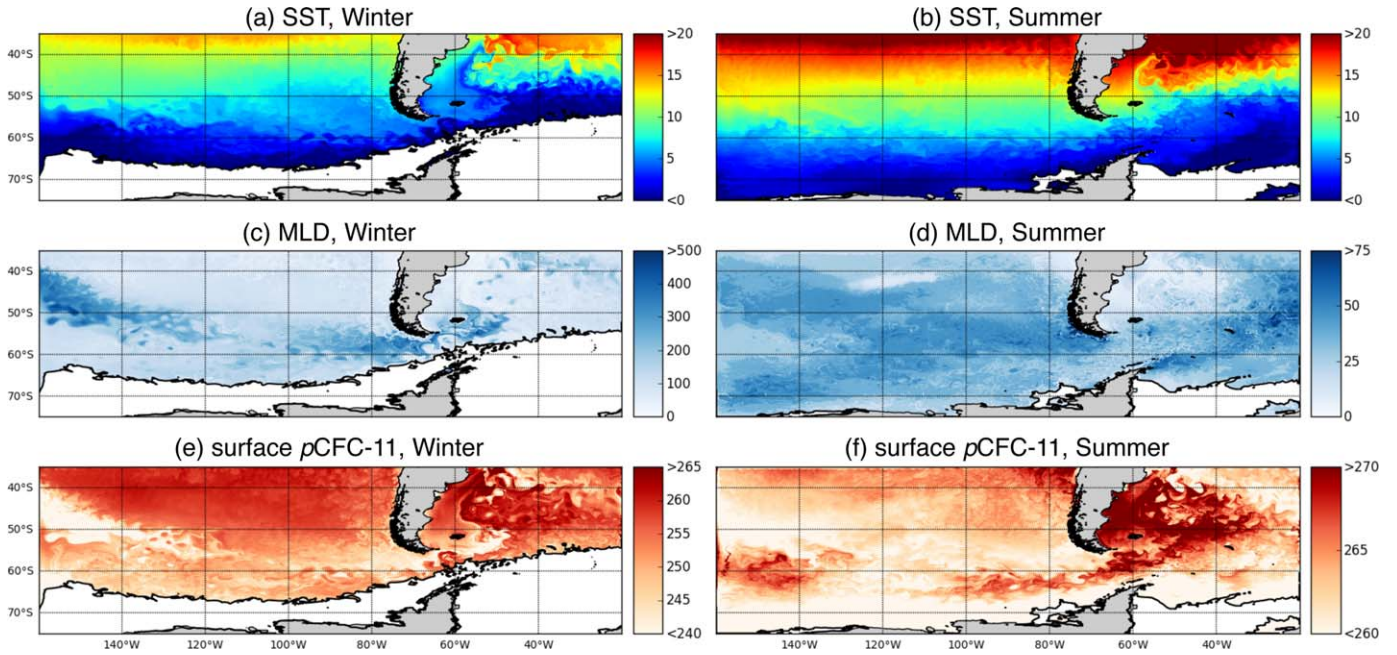

Figure 2. Snapshot of (a, b) SST, (c, d) MLD, and (e, f) surface pCFC-11 in the (left column) wintertime and (right column) summertime. Areas marked in white represent sea ice.

between C_{sat} and C. When the ocean is saturated in CFC-11, C_{sat} and C are identical and the same amount of CFC-11 leaves the ocean as enters it. However, the atmospheric *p*CFC-11 shows an increasing trend until about 1994, leading to uptake of CFC-11 by the ocean. If mesoscale eddies disturb C, then there will be changes in CFC-11 flux. In this study, we examine the anomalous CFC-11 flux induced by mesoscale eddies that are simulated in the high-resolution numerical model.

2.3. Eddy-Centric Analysis

We use sea surface height (SSH) anomalies to detect mesoscale eddies following *Chelton et al*. [2011]. If the SSH anomaly contour is closed and a series of criteria are met (as outlined in Appendix B), then it is identified as an eddy. The anomaly is computed by removing the spatial mean of the 200 $\times$ 100 km box around the model grid point. This box has a longer length in the zonal direction (200 km) than in the meridional direction (100 km) because oceanic variables typically vary less in the zonal direction. These scales are somewhat larger than the spatial decorrelation scale, which is 85 km in the Southern Ocean [*Gille and Kelly*, 1996]. Figure 1 shows detected eddies and their trajectories during 2 months in winter. High eddy activity can be seen along the ACC, which is consistent with the satellite observations [*Tulloch et al*., 2014]. Although eddies with long trajectories tend to show eastward propagation as in observations [*Chelton et al*., 2011; *Zhang et al*., 2014], directionality of eddy movements is highly variable.

Once eddies are detected from 24 SSH anomaly snapshots over a 2 month interval, their polarity, intensity, and size are also computed. For the eddy size, we adopt the concept of the speed-based definition of the eddy scale L_s [*Chelton et al*., 2011], defined as the radius of the circle with area equal to that enclosed by the SSH contour along which the surface current velocity is maximum. A total of 4681 anticyclonic and 4158 cyclonic eddies were identified in the 24 snapshots. The average L_s of eddies in our simulation is 47.3 km with standard deviation of 20 km. Composite averages of anomaly fields are then computed separately for cyclones and anticyclones in eddy-centric coordinates. The eddy-centric anomaly fields are horizontally normalized by L_s and interpolated onto a high-resolution grid spanning $\pm 2L_s$.

3. Results

3.1. Vertical Structure for Mesoscale Eddies

Anticyclones and cyclones are associated with different surface and subsurface properties. Mean vertical cross sections of simulated wintertime anticyclones and cyclones are shown in Figure 3. In the Southern Hemisphere, eddies with positive SSH generate counterclockwise-rotating currents (anticyclones) with mean velocities approaching 0.35 m s^{-1} (Figures 3a–3d). Isopycnals bend downward and the mixed layers are anomalously deep. Anticyclones are characterized by temperatures that are approximately 1.5°C warmer and salinities approximately 0.15 psu saltier than the mean. While the temperature anomaly is positive in the top 800 m, the salinity anomaly becomes negative at depth, on average, below the 27.1 isopycnal (Figures 3a and 3b). At the surface, the *p*CFC-11 anomaly is negative, becoming positive below 100 m (Figure 3c). Anticyclones have enhanced vertical mixing at the center, as evidenced by elevated vertical diffusivity (Figure 3d).

Cyclones, in contrast, rotate clockwise in the Southern Hemisphere with a maximum mean speed of 0.33 m s^{-1}, and a depressed SSH (Figures 3e–3h). In cyclones, isopycnals dome upward and the mixed layer is anomalously shallow. Thus upper ocean stratification is enhanced in the cyclone. Temperature and salinity are about 1.5°C cooler and 0.15 psu fresher than the mean (Figures 3e and 3f). As in anticyclones, the salinity anomaly also changes its sign but the temperature anomaly does not. The negative salinity anomaly in the upper ocean at eddy center becomes positive at the level of the 27.3 isopycnal or about 300 m. Cyclones show positive *p*CFC-11 anomaly in the upper 100 m but negative below that level (Figure 3g). In the center of cyclones, vertical diffusivity is about 0.05 m^2 s^{-1}, roughly one third of that in anticyclones (Figure 3h). Enhanced mixing in anticyclones is consistent with increased shear associated with trapping of near-inertial motions by virtue of local perturbation of the ambient vorticity field by the eddy [e.g., *Kunze*, 1985]. The wintertime MLD anomaly is larger than in the summertime, while T and S have the same size of anomaly with an opposite sign (not shown).

The sign changes in *p*CFC-11 anomaly can be related to eddy-driven vertical displacement of the mean profile. Typical vertical profiles of *p*CFC-11 reveal higher values at the surface that decrease with depth like

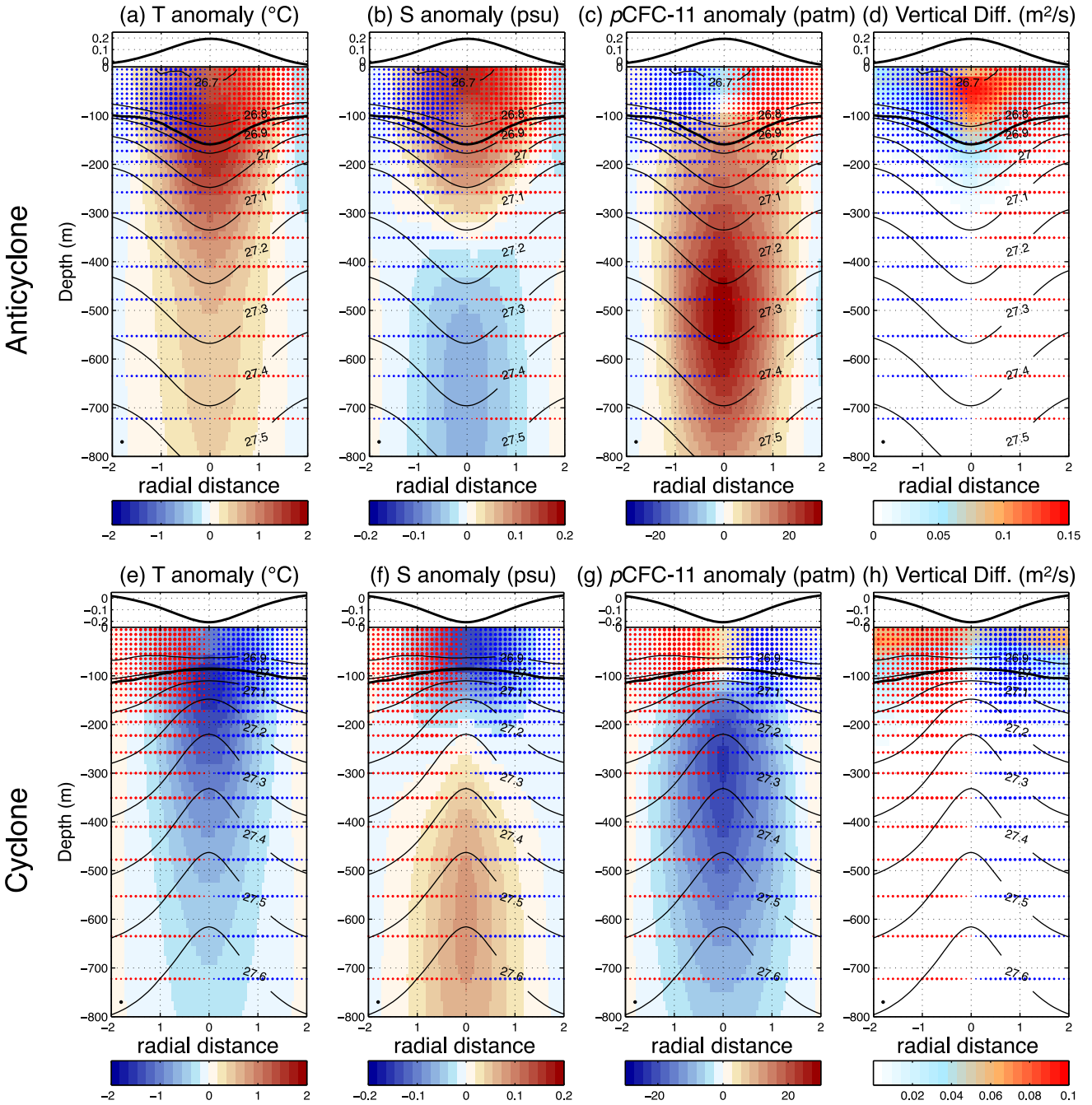

Figure 3. Mean vertical sections of temperature, salinity, *p*CFC-11 anomaly, and vertical diffusivity (shaded) in the zonal direction for (a–d) anticyclones and (e–h) cyclones in winter. Black lines on the top plots are the SSH anomaly, and thin and thick contour lines over the shaded area represent isopycnals and mixed layer depth, respectively. Meridional velocities are shown with dots over the shaded area. Red (blue) dots represent equatorward (poleward) flow with their sizes scaled by the speed. For reference, dots in the left bottom corner represent 0.3 m s^{-1}. Vertical diffusivities are computed using the KPP vertical mixing scheme. The *x* axis is normalized by L_s, the equivalent radius where the circular mean velocity is the maximum.

temperature (Figure 4). Deepening of isopycnals leads to a positive *p*CFC-11 anomaly at depth in anticyclonic eddies. On the other hand, upward displacement of isopycnals in cyclonic eddies lowers *p*CFC-11 concentration resulting in a negative anomaly. Near the surface, however, anomalies of *p*CFC-11 cannot be explained fully by the vertical displacement of isopycnals due to the presence of stronger diapycnal mixing processes.

These vertical *p*CFC-11 patterns have been seen in observations in the Southern Ocean between the tip of South Africa and the ACC [*Arhan et al.*, 2011]. In summer 2008, the GoodHope program sampled

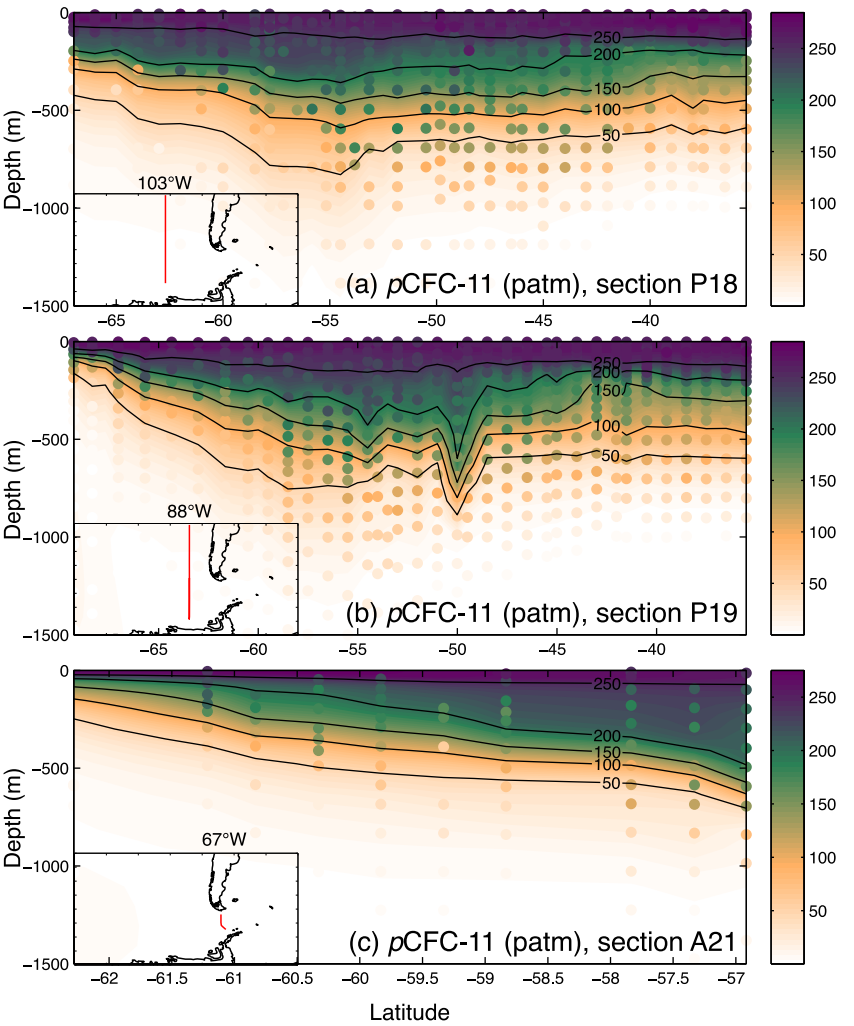

Figure 4. *p*CFC-11 (patm) from the surface to −1500 m along three meridional sections that cross through the model domain. Observed *p*CFC-11 is plotted as colored dots over that from the model simulation (shaded). The insets show the geographical location of each section.

hydrographic profiles with both physical and biogeochemical measurements collected in two eddies (one cyclonic, the other anticyclonic). Profiles in the cyclonic eddy showed anomalously higher CFC-11 in the upper 200 m with anomalously low values below. In contrast, the anticyclone had a profile of CFC-11 with anomalously low values in upper 200 m. Below that level, the CFC-11 anomaly became positive.

3.2. Cross Correlation and Eddy-Centric Analysis

In order to diagnose the relationship between mesoscale eddies and CFC flux, we correlate temperature and *p*CFC-11 anomalies at the sea surface. Both quantities are affected by the underlying eddy field as well as surface fluxes, and thus their correlation can shed light on the dynamical connection between SST and surface *p*CFC-11. In addition, we look at the cross correlation between anomalies of *p*CFC-11 and other physical variables such as net heat flux and MLD to investigate the effect of anomalous vertical mixing by mesoscale eddies on CFC-11 flux. Warm eddies can lose buoyancy to the atmosphere more quickly than cold eddies, which makes the water column in warm eddies less stable and more favorable to active vertical mixing [*Koszalka et al.*, 2010; *Kouketsu et al.*, 2012]. Moreover, trapping of near-inertial motions in anticyclones can increase shear and therefore enhance vertical mixing [*Kunze*, 1985]. The active vertical mixing in anticyclones potentially reduces the surface *p*CFC-11 concentration by blending the near-saturated surface water with unsaturated deep water. Hence, we investigate how these variables are related to *p*CFC-11 and CFC-11 flux.

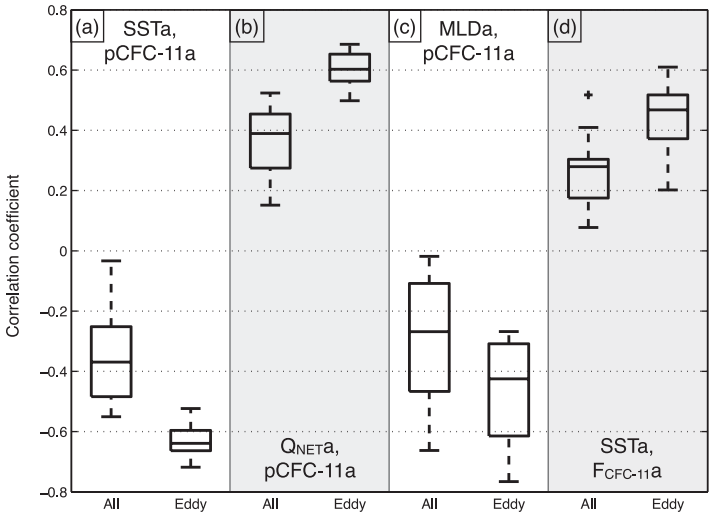

Figure 5. Cross correlation between (a) SST anomaly and surface *p*CFC-11 anomaly, (b) heat flux anomaly and surface *p*CFC-11 anomaly, (c) MLD anomaly and surface *p*CFC-11 anomaly, and (d) SST anomaly and CFC-11 flux anomaly when entire domain or just eddies are considered. The cross correlation is computed from 24 snapshots of those fields and plotted as a box plot. The line inside and the lower and upper edges of the box are the median and the 25th and 75th percentiles, respectively. Whiskers mark the boundary of approximately $\pm 2.7\sigma$. The outlier exists only in Figure 5d marked with a black cross.

3.2.1. Anomalies of SST and Surface pCFC-11

As mentioned in section 2.2, CFC-11 has a short air-sea equilibrium time scale. CFC-11 also is more soluble in cold water than in warm water [*Warner and Weiss*, 1985]. However, the temperature dependence of solubility is taken into consideration by converting it to *p*CFC-11. Surface *p*CFC-11 meridional gradients are quite different than those of SST (Figure 2). Nevertheless, their anomalies show a statistically significant cross correlation: the median of the cross correlation coefficient is −0.37 averaged over the model domain (Figure 5a). SST and surface *p*CFC-11 anomalies are more strongly correlated in winter (−0.5) than summer (−0.25). As an active tracer, temperature can modulate the circulation, possibly leading to the negative correlation between two variables. Due to CFC-11's uniform concentration in the atmosphere and its short equilibration time scale, surface *p*CFC-11 would be nearly uniform with the absence of vertical processes, and the correlation between SST and *p*CFC-11 would be close to zero. Hence, the observed negative correlation is likely to be the result of vertical processes, especially in eddies.

The correlation coefficient between SST anomaly and surface *p*CFC-11 anomaly is higher when eddy cross correlation coefficients are computed within the outer most closed SSH anomaly contour of each eddy. The median value is −0.64 (Figure 5a), nearly twice as large as the correlation computed from the entire model domain. Negative correlation indicates that warm anticyclonic (cold cyclonic) eddies contain anomalously low (high) surface *p*CFC-11. High correlation persists throughout the year (not shown) and the range between 25th and 75th percentiles is tighter than the one computed over the entire model domain.

The composite averages clearly show the anomaly patterns in anticyclonic and cyclonic eddies for the SST anomaly (Figures 6a–6d) and surface *p*CFC-11 anomaly (Figures 6m–6p). Warm anticyclones (cold cyclones) have lower (higher) surface *p*CFC-11 values. The same anomaly patterns are observed in both summer and winter, although the anomaly signals are stronger in winter.

All composite averages of SST anomaly show spatial offsets with respect to the eddy center (Figures 6a–6d). Southwestward (northwestward) spatial offsets for anticyclones (cyclones) are consistent with observations and suggest a poleward component of heat transport associated with the eddy swirl velocities [*Hausmann and Czaja*, 2012]. Surface *p*CFC-11 anomaly composites show phase shifts in the opposite direction to that of SST anomaly (Figures 6m–6p): north eastward (south eastward) for anticyclones (cyclones), suggesting that SST anomaly is not the first-order driver for the *p*CFC-11 anomaly. Because the vertical structure of pCFC-11 anomalies is more complicated than that of temperature, it is difficult to make inferences about net meridional transport on the basis of the eddy-centric patterns alone.

3.2.2. Anomalies of Net Surface Heat Flux and pCFC-11

We define the net heat flux to be positive if the ocean receives heat from the atmosphere. In the summertime, the ocean generally receives heat from the atmosphere and a positive anomaly of net heat flux indicates more heat uptake. In contrast, the ocean loses heat to the atmosphere in winter and tends to lose more heat when the SST is anomalously warm, resulting in a negative net heat flux anomaly. Regardless of season, a positive net heat flux anomaly results in more stable surface ocean and the anomalies of net heat flux and surface *p*CFC-11 are positively correlated (Figure 5b). Eddy-only correlations were significantly

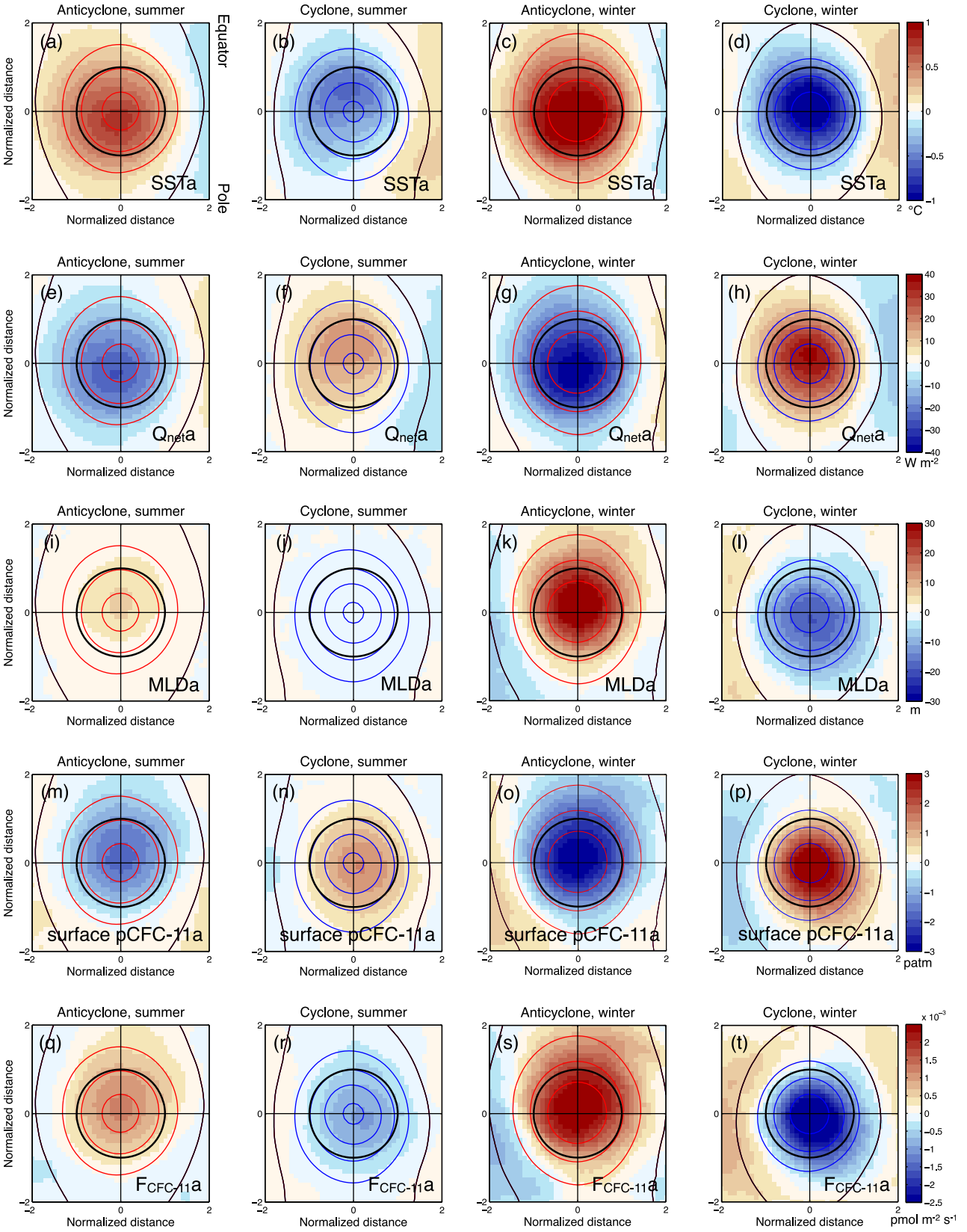

Figure 6. Eddy-centric composite averages for (a–d) SST anomaly, (e–h) heat flux anomaly, (i–l) MLD anomaly, (m–p) surface *p*CFC-11 anomaly, and (q–t) CFC-11 flux anomaly. From the left to right: columns represents anticyclonic eddy in summer, cyclonic eddy in summer, anticyclonic eddy in winter, and cyclonic eddy in winter. The contours in each plot are SSH anomaly with 5 cm interval. The black contour is the zero SSH anomaly. The thick black circle in each plot marks L_s.

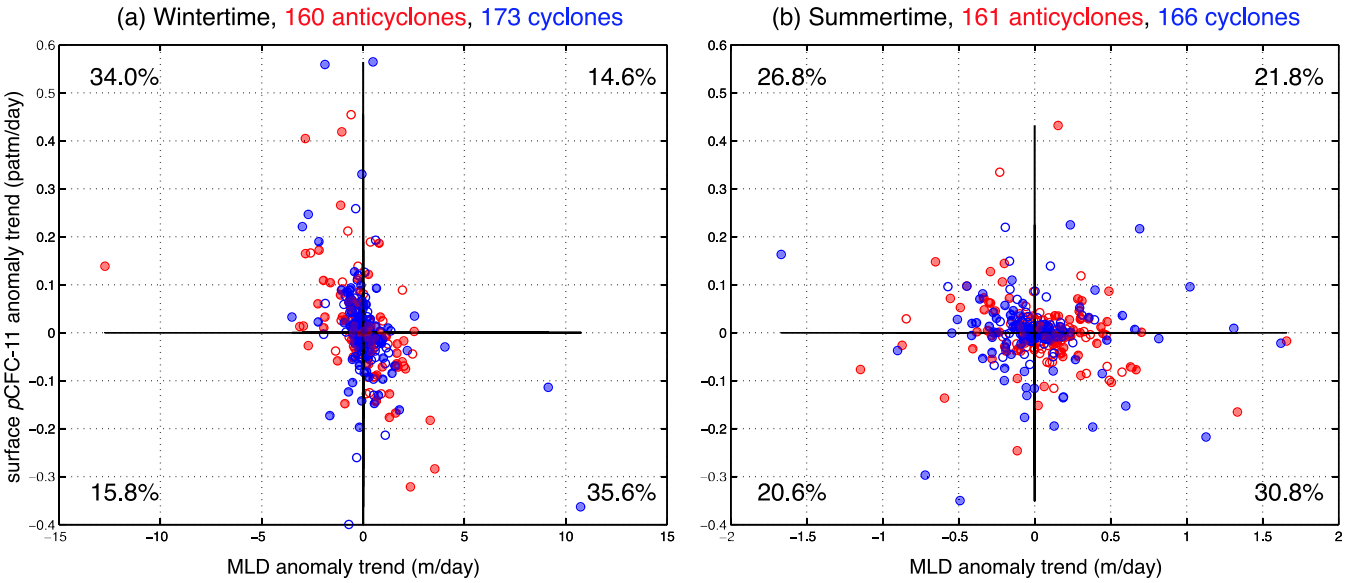

Figure 7. Trend in MLD and surface *p*CFC-11 in the eddies. Anticyclones (red) and cyclones (blue) are tracked for 2 months in both the (left) wintertime and (right) summertime. The trends are computed after linearly fitting the variables' daily anomalies. Filled dots represent the eddies with $r^2 > 0.7$. Numbers at each corner of the figures are the percentage of eddies that show the four possible combinations of trends in MLD and surface *p*CFC-11 anomaly.

greater (Figure 5b) and exhibit less seasonal variability (not shown). Anticyclonic (cyclonic) eddies are characterized by negative (positive) anomalies (Figures 6e–6h) because of their anomalous SST patterns (Figures 6a–6d). The net heat flux anomalies are greater in winter because of stronger anomalies in SST.

3.2.3. Anomalies of MLD and Surface pCFC-11

A deeper mixed layer is likely associated with weaker ambient stratification, and anomalously low surface *p*CFC-11, which results in negative cross correlation between anomalies of MLD and *p*CFC-11. A tighter correlation can be found when only eddies are considered (Figure 5c), and there is stronger seasonal variability with the coefficient being −0.61 in winter and −0.32 in summer. MLD itself shows high seasonality in the Southern Ocean, being deepest in winter and the shallowest in summer [*Dong et al.*, 2008; *Sallée et al.*, 2010b, 2010a]. As suggested in section 3.2.2, convection is restricted in summer due to warming and upper ocean stratification. In the summertime, mesoscale eddies modulate convection less than during winter (model result not shown), and so the correlations between MLD anomaly and *p*CFC-11 anomaly are relatively weak. In contrast, the ocean loses heat to the atmosphere in winter and active convection occurs with stronger wind forcing than in summer.

Eddy-centric composite averages of MLD anomaly (Figures 6i–6l) clearly show that the anomaly is greater in winter than in summer and higher amplitude in anticyclones than in cyclones. Deeper MLD in anticyclones corresponds to lower surface *p*CFC-11 in both seasons. In the wintertime, shallower MLD in cyclones is associated with positive surface *p*CFC-11 anomaly, but no clear signal is found in summer when the MLD anomaly is small (about 2 m). As seen in Figures 6k and 6l, composite averages for MLD anomaly in the wintertime also exhibit a spatial offset with respect to the eddy center, but, interestingly, the shift is opposite to that of the SST anomaly. Similarity of the spatial offset pattern between MLD and surface *p*CFC-11 anomalies suggest that surface *p*CFC-11 anomalies are primarily affected by vertical mixing in winter (Figures 6i–6p).

If vertical mixing regulates the surface *p*CFC-11, we expect to find decreasing trend of surface *p*CFC-11 anomaly with deepening MLD, or vice versa. Indeed, a negative correlation between these two trends is observed in about 70% of all eddies in winter ($r = -0.42$; Figure 7a). In contrast, no clear relationship between MLD and surface *p*CFC-11 appears in summer ($r = -0.12$; Figure 7b).

3.2.4. Anomalies of SST and CFC-11 Flux

The cross correlation between anomalies in SST and CFC-11 uptake is positive (Figure 5d), suggesting that warm (cold) eddies uptake more (less) CFC-11. As for other variables, the correlation becomes stronger if only eddies are considered.

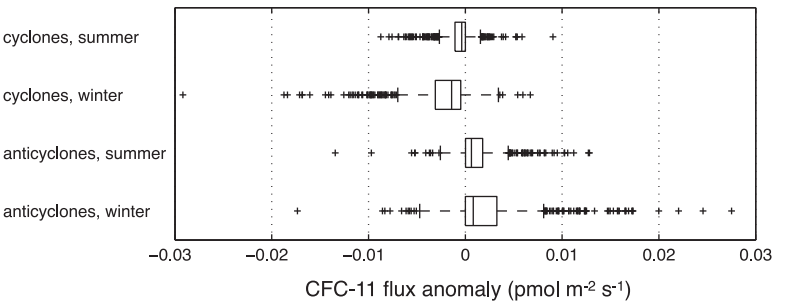

Figure 8. Distributions of CFC-11 flux anomaly in mesoscale eddies are plotted using box plots as in Figure 5. In summer, 2200 cyclones and 2187 anticyclones are used, and 1675 cyclones and 1723 anticyclones are used in winter. Black crosses represent data outside of the boundary of $[q_{0.25}-3\times(q_{0.75}-q_{0.25}), q_{0.75}+3\times(q_{0.75}-q_{0.25})]$, where $q_{0.25}$ and $q_{0.75}$ are the 25th and 75th percentiles, respectively.

Figures 6q–6t show composite averages of CFC-11 flux anomaly. Warm anticyclonic (cold cyclonic) eddies take up more (less) CFC-11, and the intensity of CFC-11 flux anomaly in both cyclones and anticyclones is stronger in winter. As suggested by (1), the structure of CFC-11 flux anomaly resembles that of the surface *p*CFC-11, showing northeastward (southeastward) spatial offsets for anticyclones (cyclones).

The CFC-11 flux anomaly in mesoscale eddies is statistically consistent. Upper quartiles for cyclones are negative, and lower quartiles for anticyclones are positive in both summer and winter (Figure 8), meaning that three out of four eddies have the same anomaly patterns shown in Figures 6q–6t. The wintertime anomalies are generally stronger in magnitude and wider in distribution. Anomalies of CFC-11 flux in cyclones and anticyclones are skewed to more negative and positive values, respectively. The wintertime CFC-11 flux anomalies in eddies are more skewed than in the summertime, suggesting a higher probability of finding significant modification of *p*CFC-11 by eddies, which is consistent with higher spatial variability of MLD in the wintertime.

3.3. Net Effect in CFC-11 Flux by Eddies

In the previous subsection, we showed that anticyclonic and cyclonic eddies contain CFC-11 flux anomalies of opposite sign. Then one naturally asks: what is the net effect of eddies on CFC-11 uptake?

Within the model domain, anticyclonic eddies take up about 23% more CFC-11 than cyclonic eddies do from 1991 to 1994 (7.02×10^6 mol versus 5.71×10^6 mol, in Table 1). With their deeper MLD and stronger vertical mixing, anticyclones efficiently reduce the surface *p*CFC-11 concentration, allowing for more CFC-11 to be taken up by the ocean. When the total CFC-11 flux is partitioned into its mean and anomaly components, the anomaly due to anticyclonic eddies is 0.78×10^6 mol (12.5% of the mean), while that due to cyclonic eddies is -0.68×10^6 mol (10.6% of the mean). These two anomalies are not completely compensating and there is a positive net effect by mesoscale eddies in CFC-11 uptake.

The net positive CFC-11 uptake is associated with nonlinear boundary layer vertical mixing. Since anticyclonic eddies occupy a broader area than cyclonic eddies (Table 1), we normalize the anomaly by the total area occupied by eddies. The net is still positive. When this anomaly is further normalized by the SSH anomaly, the net CFC-11 uptake remains positive. This suggests that the positive net effect of CFC-11 uptake is not simply a result of differences in the sizes and amplitudes of cyclones versus anticyclones, but is the result of difference of nonlinear vertical mixing in the ocean boundary layer. Greater MLD anomaly in anticyclones (Figures 6k and 6l) also suggests that asymmetry of CFC-11 flux is related to the vertical mixing.

Table 1. Total Areas Occupied by Eddies From 24 Snapshots Together With the F_{CFC-11} and F_{CFC-11} Anomaly ($F_{CFC-11}a$) Integrated Over Those Areas[a]

	Anticyclone	Cyclone	Net
Total area (km^2)	2.04×10^8	1.99×10^8	
Mean amplitude (m)	0.257	−0.265	
F_{CFC-11} (mol)	7.02×10^6	5.71×10^6	
$F_{CFC-11}a$ (mol)	0.78×10^6	-0.68×10^6	0.1×10^6
$F_{CFC-11}a$ per area (mol km^{-2})	9.78×10^{-2}	-8.69×10^{-2}	1.09×10^{-2}
$F_{CFC-11}a$ per area per amplitude (mol km^{-2} m^{-1})	0.40	−0.34	0.061

[a]The F_{CFC-11} anomaly is then normalized by the eddy area and finally by the eddy area and amplitude.

How significant is this net positive CFC-11 uptake? In order to answer this question, we

decompose the total area of each model snapshot into the fraction covered by cyclones, anticyclones, and the interstitial space. The total CFC-11 that enters the ocean over the 4 year period is 18.79×10^6 mol integrated over the model domain. When the CFC-11 flux associated with anticyclonic eddies is replaced by the interstitial mean, the total flux becomes 18.40×10^6 mol, which is 2.1% less uptake. In contrast, the total CFC-11 flux is 1.9% greater (19.15×10^6 mol) when negative anomalies associated with cyclones are replaced by the mean interstitial value. When the CFC-11 flux over all eddies is replaced by the interstitial mean value, the total flux becomes 18.71×10^6. This indicates that the net positive CFC-11 uptake by mesoscale eddies contributes to the total CFC-11 uptake by less than 0.5%. In other words, one would not expect to see a significant change in the total CFC-11 uptake with resolved mesoscale eddies because anomalies of opposite sign partially compensate for each other. We note that this does not imply that resolving eddies always has little effect on CFC-11 uptake—indeed, the eddy-driven components of the flux span from $+12.5\%$ in anticyclones to -10.6% in cyclones with respect to the mean. Moreover, resolving eddies can significantly change the time-mean circulation, and this in itself can result in notable differences in CFC-11 uptake compared with noneddy-resolving simulations with parameterized eddies. However, modulation of the flux on the scale of the eddies nearly cancels out in the calculations presented here.

4. Discussion and Conclusions

Mesoscale eddies modulate surface properties leading to anomalies in the partial pressure of CFC-11 (*p*CFC-11) and CFC-11 uptake. Warm eddies (anticyclones) become less stratified by either gaining less heat from the atmosphere in summer or losing more heat in winter along with enhanced mixing by trapping of near-inertial motions. For a given energy input, diapycnal diffusivity is enhanced down to deeper depths, and the surface *p*CFC-11 value goes down as the surface water with high *p*CFC-11 is mixed with low *p*CFC-11 subsurface water. The uptake of CFC-11 is determined by the gradient of *p*CFC-11 between the atmosphere and ocean. As the gradient of *p*CFC-11 between air and sea is enhanced, anticyclones will have anomalously large CFC-11 uptake. Conversely, cold eddies (cyclones) are more stratified. With less vertical mixing, the surface *p*CFC-11 becomes anomalously high, resulting in less CFC-11 uptake.

Total CFC-11 uptake by anticyclones is about 23% more than that by cyclones. This is because anticyclones have positive CFC-11 uptake anomaly while cyclones have negative one. These two anomalies do not completely cancel out, leaving a net positive effect of CFC-11 uptake by mesoscale eddies. This positive net effect is robust to normalization by eddy areas and amplitudes, suggesting that nonlinear vertical mixing processes are the main source for the asymmetry in the anomalies. The positive net CFC-11 uptake by anomalies is, however, less than 1% of total CFC-11 uptake.

There are other studies that also found the link between the vertical mixing and the CFC-11 flux. For example, *Haine and Richards* [1995] and *Shao et al.* [2013] argue that anomalous CFC-11 uptake can occur when the surface ocean is undersaturated due to strong vertical mixing. *England and Hirst* [1997] find that vertical convection is important for the CFC-11 simulation. When a parameterization was included for representing eddy effects on adiabatic transport, erroneous deep convection was limited and the bias in the simulated CFCs was reduced. *Booth and Kamenkovich* [2008] find that resolving eddies increases the CFC concentration in the bottom of the convection cell in the deep water formation regions. Higher CFC concentration in the bottom layer reduces the vertical CFC gradient and removal of surface CFC by convective mixing, leading to less CFC uptake. It is also possible that the CFC-11 flux can be changed by energy transfers that are not resolved by our model [*Richman et al.*, 2012; *Arbic et al.*, 2013].

A typical *p*CFC-11 vertical profile shows a decreasing trend with depth as CFC-11 enters the ocean through the surface. Downward displacement of isopycnals in anticyclones results in positive *p*CFC-11 anomaly, changing the sign of the anomaly with depth from negative at the surface to positive in the subsurface layers. Isopycnal doming in cyclones causes a negative anomaly in the subsurface layers, which is opposite from the surface positive anomaly. These vertical structures are observed along the GoodHope line in 2008 summer, and *Arhan et al.* [2011] attribute these structures to their remote source waters, based on other properties such as salinity and oxygen. Our numerical simulation reveals an alternative set of mechanisms in winter that produce a qualitatively similar pattern of anomalies: mesoscale variations in mixed layer depth modulate the *p*CFC-11 anomaly at the surface, with isopycnal displacements driving subsurface anomalies. This argument is supported by the similarity in the eddy-centric composite average anomalies of

MLD, *p*CFC-11, and CFC-11 flux (tendency toward an eastward component to their spatial offset), and the negatively correlated trend of MLD and surface *p*CFC-11 anomalies.

The simulation described herein pertains to the time period when CFC-11 concentrations in the atmosphere were increasing. After 1994, atmospheric concentrations began to stabilize and then decrease. Although the mean air-sea gradient was reduced, the role of mesoscale eddies in CFC-11 flux is unlikely to be dramatically different. Assuming that the sense of the vertical gradient of CFC-11 in this region of the ocean will remain the same (concentrations decreasing with depth), enhanced vertical mixing in anticyclones will lead to lower surface ocean pCFC-11, thereby lowering the air-sea gradient and associated flux into the atmosphere. In contrast, reduced vertical mixing in cyclones will lead to higher surface ocean pCFC-11, thereby increasing the air-sea gradient and associated flux into the atmosphere. Again, these effects will tend to compensate for each other, but quantification of the eddy-driven fluctuations in CFC-11 flux and their net effects would require explicit simulation in the new regime. This eddy-centric analysis could also be applied to investigate the role of mesoscale processes on the air-sea exchange of other gases, but care should be taken in so doing because of the differences in chemical properties, large-scale distributions, as well as the associated sources and sinks.

Appendix A: Details of the Model Settings

The boundary condition for current and tracers are prepared using the MITgcm global model run (roughly 1° horizontal resolution), closely following the configuration described in *Marshall et al.* [2014]. Once a steady state is reached with the normal year Common Ocean-ice Reference Experiments version 2 (CORE-II) surface forcing, we assume that this is the year 1900. The ocean states are further integrated for another 48 years with the CFC-11 forcing starting in the 1930s [*Walker et al.*, 2000]. Interannual atmospheric CFC-11 forcing is uniform in space in each hemisphere with linear interpolation between 10°S and 10°N. This global model is integrated for another 60 years from 1948 to 2007 with interannually varying CORE-II surface forcing that follows the experimental protocol described in *Danabasoglu et al.* [2014].

The 1/20° regional model is then integrated for 5 years from 1990 to 1994 with the CORE-II surface forcing using boundary conditions extracted from the monthly averaged fields of the global run. It is worth noting that the forcing and boundary conditions are different from those in *Tulloch et al.* [2014]. Although the simulated *p*CFC distribution is in general agreement with observations, modeled concentration is too low between 60°S and 40°S along the section P18 and P19 (Figures 4a and 4b). This is linked to the shallow mixed layer bias and weaker intermediate water formation in these regions (not shown). In section A21 across the Drake Passage, simulated *p*CFC-11 concentrations in the upper 300 m toward the north of the section are too high (Figure 4c). These model biases, however, should not introduce a limitation in analyzing the modulation of CFC-11 uptake by anticyclones and cyclones from the mean states.

Appendix B: Criteria for Detecting Mesoscale Eddies

Detecting eddies based on SSH anomaly has been performed in other studies [*Fang and Morrow*, 2003; *Chaigneau et al.*, 2008; *Chelton et al.*, 2011; *Zhang et al.*, 2014]. In this study, eddies are identified by closed SSH anomaly contours, using a criteria that is similar to that described in *Chelton et al.* [2011]. We further restrict our definition to eddies with sizes ranging from 100 to 5000 pixels, and one local SSH anomaly maximum for an anticyclone or minimum for a cyclone. One-hundred pixels roughly correspond to the area of a circle whose radius is 0.4°. Also, the minimum amplitude of the SSH anomaly for a detected eddy must be greater than 5 cm, and the maximum distance between grid points within the eddy should not exceed 300 km so that its shape is not very different from a circle.

The eddy detecting algorithm has the following procedure:

1. Loop through the SSH anomaly contours to find the closed ones.
2. Examine how many pixels are in each closed contour. If there are appropriate numbers, then proceed.
3. Check if there is only one extreme value. If so, then proceed.
4. Check if the amplitude of the eddy is big enough. If so, then proceed.
5. Compute the maximum distance between pixels. If this is shorter than 300 km, this is defined as an eddy.

We evaluated the SSH above algorithm with an independent automated eddy detection method based on the geometry of the velocity vectors [*Nencioli et al*., 2010]. The latter algorithm finds eddies using the raw velocity field, hence is not sensitive to the method of computing anomaly described in section 2.3. Eddies detected by the two methods are comparable, indicating that our results should not be sensitive to the details of eddy tracking procedure.

Acknowledgments
The MITgcm can be obtained from http://mitgcm.org. The surface forcing data used in this study are available at the Geophysical Fluid Dynamics Laboratory data portal webpage (http://data1.gfdl.noaa.gov/nomads/forms/core/COREv2.html). We gratefully acknowledge NSF support of the MOBY project (grant OCE-1048926 to MIT and OCE-1048897 to WHOI). In addition, P.G. and D.J.M. thank NASA for partial support of this work through grant NNX13AE47G. The authors would like to thank two anonymous reviewers for valuable comments and suggestions, which significantly improved the manuscript.

References

Adcroft, A., C. Hill, and J. Marshall (1997), Representation of topography by shaved cells in a height coordinate ocean model, *Mon. Weather Rev.*, *125*, 2293–2315.
Adcroft, A. J., C. N. Hill, and J. C. Marshall (1999), A new treatment of the Coriolis terms in C-grid models at both high and low resolutions, *Mon. Weather Rev.*, *127*, 1928–1936.
Arbic, B. K., K. L. Polzin, R. B. Scott, J. G. Richman, and J. F. Shriver (2013), On eddy viscosity, energy cascades, and the horizontal resolution of gridded satellite altimeter products, *J. Phys. Oceanogr.*, *43*, 283–300.
Arhan, M., S. Speich, C. Messager, G. Dencausse, R. Fine, and M. Boye (2011), Anticyclonic and cyclonic eddies of subtropical origin in the subantarctic zone south of Africa, *J. Geophys. Res.*, *116*, C11004, doi:10.1029/2011JC007140.
Booth, J., and I. Kamenkovich (2008), Isolating the role of mesoscale eddies in mixing of a passive tracer in an eddy resolving model, *J. Geophys. Res.*, *113*, C05021, doi:10.1020/2007JC004510.
Chaigneau, A., A. Gizolme, and C. Grados (2008), Mesoscale eddies off Peuro in altimeter records: Identification algorithms and eddy spatio-temporal patterns, *Prog. Oceanogr.*, *79*, 106–119, doi:10.1016/j.pocean.2008.10.013.
Chelton, D., M. Schlax, and R. Samelson (2011), Global observations of nonlinear mesoscale eddies, *Prog. Oceanogr.*, *91*(2), 167–216.
Danabasoglu, G., et al. (2014), North Atlantic simulations in coordinated ocean-ice reference experiments phase II (CORE-II). Part I: Mean states, *Ocean Modell.*, *73*, 76–107, doi:10.1016/j.ocemod.2013.10.005.
Dixon, K. W., J. L. Bullister, R. H. Gammon, and R. J. Stouffer (1996), Examining a coupled climate model using CFC-11 as an ocean tracer, *Geophys. Res. Lett.*, *23*(15), 1957–1960.
Dong, S., J. Sprintall, S. T. Gille, and L. Talley (2008), Southern Ocean mixed-layer depth from Argo float profiles, *J. Geophys. Res.*, *113*, C06013, doi:10.1029/2006JC004051.
Dutay, J. C., et al. (2002), Evaluation of ocean model ventilation with CFC-11: Comparison of 13 global ocean models, *Ocean Modell.*, *4*, 89–120.
England, M. H. (1995), Using chlorofluorocarbons to assess ocean climate models, *Geophys. Res. Lett.*, *22*(22), 3051–3054.
England, M. H., and A. C. Hirst (1997), Chlorofluorocarbon uptake in a World Ocean model: 2. Sensitivity to surface thermohaline forcing and subsurface mixing parameterisation, *J. Geophys. Res.*, *102*(C7), 15,709–15,731.
England, M. H., and E. Maier-Reimer (2001), Using chemical tracers to assess ocean models, *Rev. Geophys.*, *39*(1), 29–70.
Fang, F., and R. Morrow (2003), Evolution, movement and decay of warm-core Leeuwin Current eddies, *Deep Sea Res., Part II*, *50*, 2245–2261, doi:10.1016/s0967-0645(03)00055-9.
Fine, R. A. (2011), Observations of CFCs and SF6 as ocean tracers, *Annu. Rev. Mar. Sci.*, *3*, 173–195.
Gaube, P., D. B. Chelton, P. G. Strutton, and M. J. Behrenfeld (2013), Satellite observations of chlorophyll, phytoplankton biomass, and Ekman pumping in nonlinear mesoscale eddies, *J. Geophys. Res. Oceans*, *118*, 6349–6370, doi:10.1002/2013JC009027.
Gille, S. T., and K. A. Kelly (1996), Scales of spatial and temporal variability in the southern ocean, *J. Geophys. Res.*, *101*(C4), 8759–8773.
Gruber, N., Z. Lachkar, H. Frenzel, P. Marchesiello, M. Münnich, J. C. McWilliams, T. Nagai, and G.-K. Plattner (2011), Mesoscale eddy-induced reduction in eastern boundary upwelling systems, *Nat. Geosci.*, *4*, 787–792, doi:10.1038/ngeo1273.
Haine, T. W. N., and K. J. Richards (1995), The influence of the seasonal mixed-layer on oceanic uptake of CFCs, *J. Geophys. Res.*, *100*(C6), 10,727–10,744.
Hartin, C. A., R. A. Fine, B. M. Sloyan, L. D. Talley, T. K. Chereskin, and J. Happell (2011), Formation rates of subantarctic mode water and Antarctic intermediate water within the South Pacific, *Deep Sea Res., Part I*, *58*, 524–534.
Hausmann, U., and A. Czaja (2012), The observed signature of mesoscale eddies in sea surface temperature and the associated heat transport, *Deep Sea Res., Part I*, *70*, 60–72.
Ito, T., J. Marshall, and M. Follows (2004), What controls the uptake of transient tracers in the southern ocean?, *Global Biogeochem. Cycles*, *18*, GB2021, doi:10.1029/2003GB002103.
Key, R. M., et al. (2004), A global ocean carbon climatology: Results from Global Data Analysis Project (GLODAP), *Global Biogeochem. Cycles*, *18*, GB4031, doi:10.1029/2004GB002247.
Koszalka, I., L. Ceballos, and A. Bracco (2010), Vertical mixing and coherent anticyclones in the ocean: The role of stratification, *Nonlinear Process. Geophys.*, *17*, 37–47.
Kouketsu, S., H. Tomita, E. Oka, S. Hosoda, T. Kobayashi, and K. Sato (2012), The role of meso-scale eddies in mixed layer deepening and mode water formation in the western North Pacific, *J. Oceanogr.*, *68*(1), 63–77, doi:10.1007/s10872-011-0049-9.
Kunze, E. (1985), Near-inertial wave propagation in geostrophic shear, *J. Phys. Oceanogr.*, *15*, 544–565.
LaCasce, J. H., R. Ferrari, J. Marshall, R. Tulloch, D. Balwada, and K. Speer (2014), Float-derived isopycnal diffusivities in the DIMES experiment, *J. Phys. Oceanogr.*, *44*, 764–780.
Lachkar, Z., J. C. Orr, J. C. Dutay, and P. Delecluse (2007), Effects of mesoscale eddies on global ocean distributions of CFC-11, CO_2, and $\delta^{14}C$, *Ocean Sci.*, *3*, 461–482.
Lathuilière, C., V. Echevin, M. Lévy, and G. Madec (2010), On the role of the mesoscale circulation on an idealized coastal upwelling ecosystem, *J. Geophys. Res.*, *115*, C09018, doi:10.1029/2009JC005827.
Long, M. C., K. Lindsay, S. Peacock, J. K. Moore, and S. C. Doney (2013), Twentieth-century oceanic carbon uptake and storage in CESM1(BGC), *J. Clim.*, *26*, 6775–6800.
Marshall, J., A. Adcroft, C. Hill, L. Perelman, and C. Heisey (1997a), A finite-volume, incompressible Navier Stokes model for studies of the ocean on parallel computers, *J. Geophys. Res.*, *102*(C3), 5753–5766.
Marshall, J., C. Hill, L. Perelman, and A. Adcroft (1997b), Hydrostatic, quasi-hydrostatic, and nonhydrostatic ocean modeling, *J. Geophys. Res.*, *102*(C3), 5733–5752.
Marshall, J., H. Jones, and C. Hill (1998), Efficient ocean modeling using non-hydrostatic algorithms, *J. Mar. Syst.*, *18*, 115–134.
Marshall, J., K. Armour, J. Scott, Y. Kostov, U. Hausmann, D. Ferreira, T. Shepherd, and C. Bitz (2014), The ocean's role in polar climate change: Asymmetric Arctic and Antarctic responses to greenhouse gas and ozone forcing, *Philos. Trans. R. Soc. A*, *372* 20130040.

McGillicuddy, D. J., A. R. Robinson, D. A. Siegel, H. W. Jannasch, R. Johnson, T. D. Dickey, J. McNeil, A. F. Michaels, and A. H. Knap (1998), New evidence for the impact of mesoscale eddies on biogeochemical cycling in the Sargasso Sea, *Nature*, *394*, 263–266.

McGillicuddy, D. J., et al. (2007), Eddy/wind interactions stimulate extraordinary mid-ocean plankton blooms, *Science*, *316*, 1021–1026.

Müller, S. A., F. Joos, N. R. Edwards, and T. F. Stocker (2006), Water mass distribution and ventilation time scales in a cost-efficient, three-dimensional ocean model, *J. Clim.*, *19*, 5479–5499.

Nencioli, F., C. Dong, T. Dickey, L. Washburn, and J. McWilliams (2010), A vector geometry based eddy detection algorithm and its application to a high-resolution numerical model product and high-frequency radar surface velocities in the Southern California Bight, *J. Atmos. Oceanic Technol.*, *27*, 564–579.

Oschlies, A. (2002), Nutrient supply to the surface waters of the North Atlantic: A model study, *J. Geophys. Res.*, *107*(C5), 3046, doi:10.1029/2000JC000275.

Richman, J. G., B. K. Arbic, J. F. Shriver, E. J. Metzler, and A. J. Wallcraft (2012), Inferring dynamics from the wavenumber spectra of an eddying global ocean model with embedded tides, *J. Geophys. Res.*, *117*, C12012, doi:10.1029/2012JC008364.

Sallée, J.-B., K. Speer, and S. Rintoul (2010a), Zonally asymmetric response of the Southern Ocean mixed-layer depth to the southern annular mode, *Nat. Geosci.*, *3*, 273–279.

Sallée, J.-B., K. Speer, S. Rintoul, and S. Wijffels (2010b), Southern Ocean thermocline ventilation, *J. Phys. Oceanogr.*, *40*, 509–529, doi:10.1175/2009JPO4291.1.

Shao, A. E., S. Mecking, L. Thompson, and R. E. Sonnerup (2013), Mixed layer saturations of CFC-11, CFC-12, and SF_6 in a global isopycnal model, *J. Geophys. Res. Oceans*, *118*, 4978–4988, doi:10.1002/jgrc.20370.

Trossman, D. S., L. Thompson, S. Mecking, and M. J. Warner (2012), On the formation, ventilation, and erosion of mode waters in the North Atlantic and Southern Oceans, *J. Geophys. Res.*, *117*, C09026, doi:10.1029/2012JC008090.

Tulloch, R., et al. (2014), Direct estimates of lateral eddy diffusivity upstream of Drake Passage, *J. Phys. Oceanogr.*, *44*, 2593–2616.

Walker, S. J., R. F. Weiss, and P. K. Salameh (2000), Reconstructed histories of the annual mean atmospheric mole fractions for the halocarbons CFC-11 CFC-12, CFC-113, and carbon tetrachloride, *J. Geophys. Res.*, *105*(C6), 14,285–14,296, doi:10.1029/1999JC900273.

Wanninkhof, R. (1992), Relationship between wind speed and gas exchange over the ocean, *J. Geophys. Res.*, *97*(C5), 7373–7382, doi:10.1029/92JC00188.

Warner, M., and R. Weiss (1985), Solubilities of chlorofluorocarbons 11 and 12 in water and seawater, *Deep Sea Res., Part A*, *32*(12), 1485–1497, doi:10.1016/0198-0149(85)90099-8.

Waugh, D. W., F. Primeau, T. DeVrise, and M. Holzer (2013), Recent changes in the ventilation of the Southern Oceans, *Science*, *339*, 568–570, doi:10.1126/science.1225411.

Zhang, Z., W. Wang, and B. Qiu (2014), Oceanic mass transport by mesoscale eddies, *Science*, *345*(6194), 322–324, doi:10.1126/science.1252418.